Novel High-Performance Glyoxylate Derivative-based Photoinitiators for Free Radical Photopolymerization and 3D Printing with Visible LED

Tong Gao, Yijun Zhang, Fabrice Morlet-Savary, Bernadette Graff, Jing Zhang, Pu Xiao, Frédéric Dumur, Jacques Lalevée

Novel High-Performance Glyoxylate Derivative-based Photoinitiators for Free Radical Photopolymerization and 3D Printing with Visible LED

Tong Gao [a,b], Yijun Zhang [a,b], Fabrice Morlet-Savary [a,b], Bernadette Graff [a,b], Jing Zhang [c], Pu Xiao [d],* Frédéric Dumur [e] and Jacques Lalevée [a,b]*

[a] Université de Haute-Alsace, CNRS, IS2M UMR7361, F-68100 Mulhouse, France.
[b] Université de Strasbourg, France.
[c] Future Industries Institute, University of South Australia, Mawson Lakes, SA 5095, Australia.
[d] State Key Laboratory of High Performance Ceramics and Superfine Microstructure, Shanghai Institute of Ceramics, Chinese Academy of Sciences, Shanghai 200050, P. R. China.
[e] Aix Marseille Univ, CNRS, ICR, UMR 7273, F-13397 Marseille, France.

E-mail address: p.xiao@mail.sic.ac.cn (PX); jacques.lalevee@uha.fr (JL);

Abstract

Investigations concerning the glyoxylate moiety as a photocleavable functional group for visible light photoinitiators, particularly in the initiation of free radical photopolymerization, remains limited. This study introduces nine innovative carbazole-based ethyl glyoxylate derivatives (CEGs), synthesized and found to exhibit excellent photoinitiation abilities as monocomponent photoinitiating systems. Notably, these structures demonstrate robust absorption in the near-UV/visible range, surpassing the commercial photoinitiators. Moreover, the newly developed glyoxylate derivatives showed higher acrylate function conversions compared to MBF in free radical photopolymerization. Elucidation of the photoinitiation mechanism of CEGs was achieved through comprehensive analysis involving the decarboxylation reaction and electron spin resonance spin trapping. Furthermore, their practical utility was confirmed during direct laser write and 3D printing processes, enabling the successful fabrication of 3D printed objects. This study introduces pioneering concepts and effective strategies in molecular design of novel photoinitiators, showcasing their potential for highly advantageous applications in 3D printing.

Keywords: LED; photopolymerization; glyoxylate; Type I photoinitiator; 3D printing.

1. Introduction

Photopolymerization, a technology driving polymer synthesis through chain reactions initiated by photoinitiators (PIs) under light radiation, holds a pivotal role in polymer material science.[1] Its inherent versatility and adaptability make it a preferred technique across various commercial sectors including coatings,[2, 3] inks,[4] adhesives,[5] food packaging,[6] dentistry,[6] medicine, 3D printing[5, 7], microcircuits, and semiconductors industries.[7, 8] This widespread adoption owes to its environmental friendliness, controllability, and high efficiency.[9]

The utilization of light-emitting diodes (LEDs) as irradiation sources offers several advantages over traditional mercury lamps, encompassing safety, environmental responsibility, energy efficiency, affordability, durability, and superior effectiveness.[5] Consequently, there is a pressing demand for the development of novel PIs exhibiting exceptional reactivities when exposed to near UV and/or visible LED illumination.

Upon absorbing light energy and reaching the excited state, PIs generate active species, such as free radicals,[3, 10] anions,[11] or cations,[12] initiating the chain reaction. Depending on the photoinitiation mechanism, classical radical-based PIs can initiate free radical polymerization in two ways. Type I PIs involve cleaving a labile chemical bond upon irradiation, offering the advantage of simplified monocomponent systems for the elaboration of the photocurable resins. Type II PIs require intermolecular reactions to produce initiating species through hydrogen abstraction and typically function in multicomponent photoinitiating systems. Classically, PIs absorb light and transfer an electron and a proton from a donor/co-initiator, generating free radicals.[3, 9] Nevertheless, conventional PIs primarily absorb light below 365 nm, mismatching the emission wavelength of 405 nm LEDs (or longer wavelengths). They can also exhibit drawbacks such as strong odor, toxicity, and poor solubility in most of the photocurable resins,[13] which may affect both the polymerization efficiency and the final industrial applications. Consequently, many commercially available PIs are unsuitable for LED-initiated photopolymerization, sparking recent research focus on tailored PIs for this purpose.

Presently, commonly used PIs for LED-driven photopolymerization fall under Type II classification, lauded for their exceptional light absorption properties and versatility when combined with additives, extending their absorptions from the near-ultraviolet into the visible range. Notable examples of Type II photoinitiators include benzophenones,[14] thioxanthones,[15, 16] quinones,[17] phenothiazines,[18] curcuminoids,[19] and naphthalimides.[20] According to a hydrogen abstraction mechanism, Type II PIs work with additives such as amines to generate reactive species. However, these systems suffer from several drawbacks. For instance, this bimolecular or multicomponent approach may also result in lower initiation activity, especially in

high-viscosity formulations, where the efficiency of energy transfer as well as electron transfer between the PI and the co-initiator is influenced by diffusion.[21] In contrast, Type I PIs can directly initiate polymerization by generating reactive free radicals without the addition of any additive. This underscores the increasing need to develop Type I PIs specifically for LED-driven photopolymerization.

Previously reported Type I PIs for LED-induced photopolymerization, such as oxime esters,[22] acylphosphine oxides,[23] α-dicarbonyls,[5, 24] and naphthalimide derivatives[25] possess drawbacks including a poor solubility in monomers, a limited penetration of light, and complex synthetic routes. These drawbacks severely limit their application in thick film curing systems and 3D printing. Addressing these limitations, it is of significant importance to elaborate simple synthetic routes for the preparation of novel Type I PIs and to investigate their photoinitiation abilities to 3D printing. Methyl benzoylformate (MBF) stands as a well-researched commercial PI.[26] However, this benchmark PI lacks absorption in the visible range, primarily owing to the presence of a unique aromatic ring. Consequently, its main absorption is centered in the UV range remaining below 300 nm. The design of glyoxylate derivatives emerges as an intriguing prospect from a synthetic standpoint. Unlike oxime esters, which require a complex three-step synthesis involving acylation or formylation, oxime formation, and esterification of the oxime group, glyoxylates can be synthesized efficiently in a single step using a Friedel-Craft reaction.[27] This inherent simplicity and cost-effectiveness make glyoxylates notably more appealing structures for the development of inexpensive and easily synthesizable Type I photoinitiators compared to other families within this category.

In this study, we designed and successfully synthesized a series of carbazole-based ethyl glyoxylate derivatives (CEGs) as novel Type I PIs (Scheme 1). Carbazole's efficiency as a photosensitizer, excellent stability, and high molar extinction coefficients makes it an ideal chromophore for Type I PIs.[28] Moreover, this aromatic heterocyclic organic compound possessing a tricyclic structure is characterized by an excellent thermal, chemical and photochemical stability, making this scaffold a candidate of choice for the design of photoinitiators. Additionally, the chemistry of carbazole is well-documented, facilitating the synthesis of new derivatives.[29-31] Introduction of the carbazole scaffold into CEGs resulted in PIs with redshifted absorption compared to that of MBF, enhancing their absorption properties and photosensitivity at 405 nm. These modifications conferred impressive initiation characteristics to CEGs, making them highly suitable for 3D printing when exposed to LED irradiation.[32, 33] The photoinitiation abilities of CEGs were evaluated not only in single-component photoinitiation systems (PISs), but also in two- and three-component PISs with the addition of an amine and an iodonium salt. Real-time Fourier transform

infrared (RT-FTIR) spectroscopy was employed to assess the kinetic performance of the different photoinitiating systems during the free radical photopolymerization (FRP) of trimethylolpropane triacrylate (TMPTA) upon a 405 nm LED exposure. Comprehensive investigations of the photochemical properties and the photoinitiation mechanisms of CEGs were conducted through complementary techniques including UV-visible absorption and fluorescence spectroscopy as well as Electron Spin Resonance (ESR)-Spin Trapping experiments. Finally, 3D printing and direct laser write (DLW) tests validated the potential of these structures for practical applications.

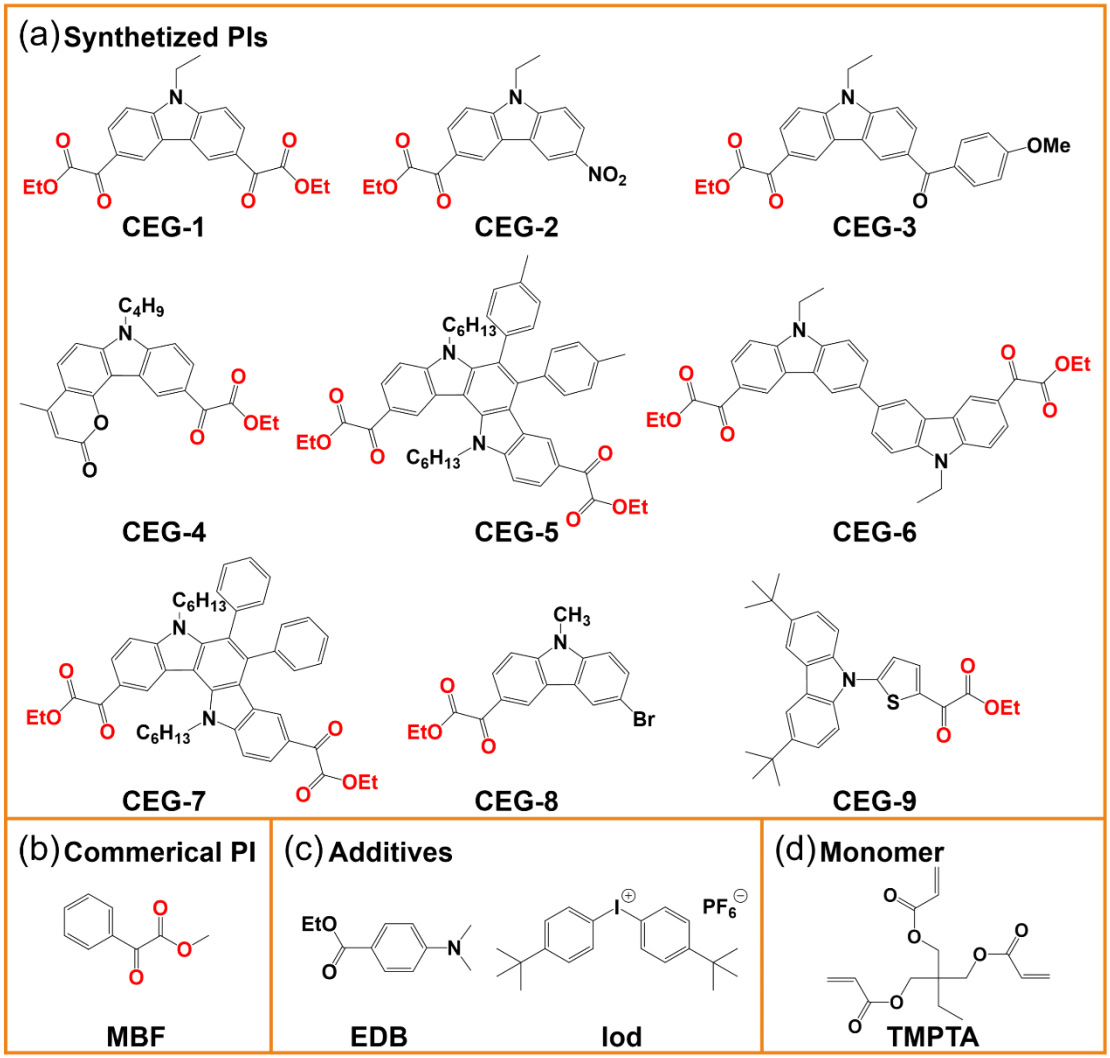

Scheme 1. Chemical structures of: (a) the synthesized ethyl glyoxylate derivatives (CEGs) containing the carbazole scaffold, (b) MBF, (c) different additives and (d) the trifunctional acrylate monomer used in this work.

2. Experimental Section

2.1 Materials

Trimethylolpropane triacrylate (TMPTA) which served as the trifunctional monomer for the free radical polymerization experiments was obtained from Sartomer-Europe (Verneuil en Halatte, France). Methyl benzoylformate (MBF) was purchased from Sigma Aldrich. *N-tert*-Butyl-α-phenylnitrone (PBN) which was used as the free radical trapping agent, *tert*-butylbenzene, acetonitrile, ethyl 4-(dimethylamino)benzoate (EDB) and di-*tert*-butylphenyliodonium hexafluorophosphate (Iod) were purchased from Sigma-Aldrich.

2.2 Synthesis of CEGs

Synthetic routes to obtain the different structural CEGs are described in Scheme 2. Details concerning the procedure and the different characterizations of CEGs are given in the Supporting Information.

2.3 Characterizations

Bruker Avance 400 spectrometer was used to record the ^{1}H NMR (400 MHz) and ^{13}C NMR (101 MHz) spectra of CEGs.

2.4 Irradiation Sources

LED (M405L2-ThorLabs) with an emission wavelength of 405 nm was used as the radiation light source. Light intensity of 110 $mW \cdot cm^{-2}$ was measured on the sample surface using a power meter (ThorLabs PM100D).

2.5 UV-visible Absorption Properties

After being dissolved in acetonitrile at a concentration of 5×10^{-5} M, CEGs were subjected to UV-visible absorption analyses employing a JASCO V730 spectrometer. Steady-state photolysis experiments were conducted with a 405 nm LED (110 $mW \cdot cm^{-2}$) as the radiation light source using the same concentration of PIs and the same apparatus as described above to measure the UV-visible absorption spectra of the PIs under various irradiation time.

2.6 Computational Procedures

Electronic absorption spectra and molecular orbitals of CEGs were calculated based on the density-functional theory at UB3LYP/6-31G* using the Gaussian 09 software package. Geometries of the ground and triplet state (T_1) as well as the bond dissociation energy (BDE), triplet state energy (E_T), and enthalpy of cleavage from T_1 (ΔH) were obtained from energy calculations.

2.7 Solubility in Monomers

Solubility of CEGs in acrylate monomers was strongly related to the activity of CEGs during the photopolymerization reactions. Each CEG was added to TMPTA separately and stirred at room temperature until complete dissolution. The solubility was calculated with the following equation:

$$S = \frac{m_{PI}}{m_{PI} + m_{TMPTA}} \times 100\% \quad (2)$$

where S was the solubility of PIs, m_{PI} was the mass of different PIs at the solubility limit, and m_{TMPTA} was the mass of TMPTA.[9, 34]

2.8 Photopolymerization Experiments

Photopolymerization kinetics of TMPTA initiated by CEGs-based photoinitiating systems were studied using RT-FTIR spectroscopy. Initiation abilities of CEGs with concentrations of 1.25×10^{-6} mol·g^{-1} in TMPTA, 2.5×10^{-6} mol·g^{-1} in TMPTA, and 1.25×10^{-5} mol·g^{-1} in TMPTA as monocomponent systems were first investigated. Photoinitiation abilities of PISs in two- and three-component PISs were also investigated. Concentrations of CEGs, EDB, and Iod were all 1.25×10^{-5} mol·g^{-1} in TMPTA. Mixtures of CEGs and TMPTA were prepared proportionally and stirred under dark conditions for 24 h. These resins were transferred in molds for thick sample (1.4 mm) polymerization experiments under air. Regarding thin samples, the photopolymerization solutions were placed in laminate between two layers of polypropylene transparent films with the thickness of 25 μm so that oxygen inhibition effect could be reduced. These photosensitive formulations were then irradiated using a 405 nm LED for 600 s. To determine the photopolymerization conversions, the area of the signal at about 1620 cm^{-1} (for thin samples) and 6150 cm^{-1} (for thick samples) were monitored over time i.e. IR spectra of the photopolymerization solutions under 405 nm LED irradiation were recorded at regular intervals. The equation below was employed to calculate the acrylate function conversions (Conv) of TMPTA at different time intervals:

$$Conv(\%) = \frac{A_0 - A_t}{A_0} \times 100\%$$

where A_0 stands for the peak area at 0 s, and A_t signifies the peak area at time t s. The photopolymerization kinetics with the addition of amine and iodonium salts were carried out according to the same method as above.

2.9 Fluorescence Experiments

CEGs at a concentration of 5×10^{-5} M were first dissolved in acetonitrile, and then recording of the fluorescence spectra of CEGs was carried out using a JASCO FP-750

spectrofluorometer. Following this, an examination of the fluorescence excited state lifetimes of CEGs was conducted with the assistance of a time-correlated single-photon counting system, a HORIBA® DeltaFlex with a HORIBA® PPD-850 as detector. To assess the impulse response function (IRF) of the instrument, a colloidal silica suspension known as LUDOX was employed. An excitation wavelength of 367 nm was chosen with a pulse duration below 1.4 ns.

2.10 Electron Spin Resonance Spin Trapping (ESR-ST) Experiments

Electron spin trapping experiments were conducted to record and detect the free radicals formed during irradiation using an ESR X-band spectrometer (Bruker EMX-Plus). In these experiments, the concentration of CEGs was 1×10^{-4} M. PBN (5×10^{-4} M) and *tert*-butylbenzene were chosen as the radical capturing agent and solvent, respectively. The light source chosen was a 405 nm LED and different CEGs were investigated under N_2 atmosphere at room temperature. Finally, the PEST WINSIM program was employed to carry out simulations of ESR spectra.

2.11 3D Printing Experiments

The photocurable formulation was prepared first (see above for the procedure). The concentration of CEGs was 1.25×10^{-5} mol·g^{-1} in TMPTA. Next, the solution was 3D printed using a 3D printer (Anycubic Photon D2) based on digital light processing (DLP) technology at 405 nm. The implementation of DLW was accomplished by employing a 405 nm laser diode. Finally, the patterns derived from the DLW were examined through the lens of a numerical optical microscope (NOM, OLYMPUS DSX-HRSU).

3. Results and Discussion

3.1 Synthesis of CEGs

The nine CEGs reported in this work contained at least one carbazole and one ethyl glyoxylate unit. The synthesis of these chemicals involved a straightforward process, outlined in Scheme 2. Notably, the carbazole-containing precursors were used as foundational materials, with the introduction of the photocleavable ethyl glyoxylate moiety achieved in a single step through a Friedel-Craft reaction. Previously reported syntheses in the literature detailed the preparation of precursors for CEG-2,[35] CEG-3,[36] CEG-4,[37] CEG-6,[38] CEG-7,[39] CEG-8,[40] and CEG-9,[41] while CEG-1 was commercially available. Specifically, the precursor for CEG-5 was synthesized for this research in two steps. Firstly, an acid-catalyzed cycloaddition of two equivalents of indole with 1,2-*bis*(4-methylphenyl)-1,2-ethanedione[42] produced 6,7-di-*p*-tolyl-5,12-dihydroindolo[3,2-*a*]carbazole. Subsequently, alkylation with iodohexane in the

presence of potassium *tert*-butoxide as the base yielded CEG-5 precursor. The reaction of these precursors with ethyl chlorooxoacetate in dichloromethane (DCM) and $AlCl_3$ as the coupling agent provided the different CEGs compounds with satisfactory yields, ranging from 66% for CEG-7 to 92% for CEG-9 as summarized in Table 1. It is worth noting that the yields for CEG-5 and CEG-7 were slightly lower than that of the other CEGs due to a more complex purification process in these instances. This observation aligned with previous literature findings. The potential for incomplete Friedel-Craft reaction in the synthesis of 5,12-dialkyl-5,12-dihydroindolo[3,2-*a*]carbazoles has been reported, , resulting in challenging separations between mono-substituted and di-substituted carbazoles.[39] The choice of ethyl chlorooxoacetate over methyl chlorooxoacetate in the synthesis process was influenced by cost considerations, as ethyl chlorooxoacetate is more economically viable. The novelty of the glyoxylate derivatives presented in this research cannot be overlooked; these compounds have not been previously published. Furthermore, the exploration of 5,12-dialkyl-5,12-dihydroindolo[3,2-*a*]carbazoles has been relatively recent, starting from 2019.[43] Similarly, only few coumarin-carbazole structures have also been reported to date in the literature,[44] an efficient synthesis of this structure being also known since only 2019. This highlights the scarcity of structures of these two families of dyes, and emphasizes the significance of investigating and understanding such chemical architectures.

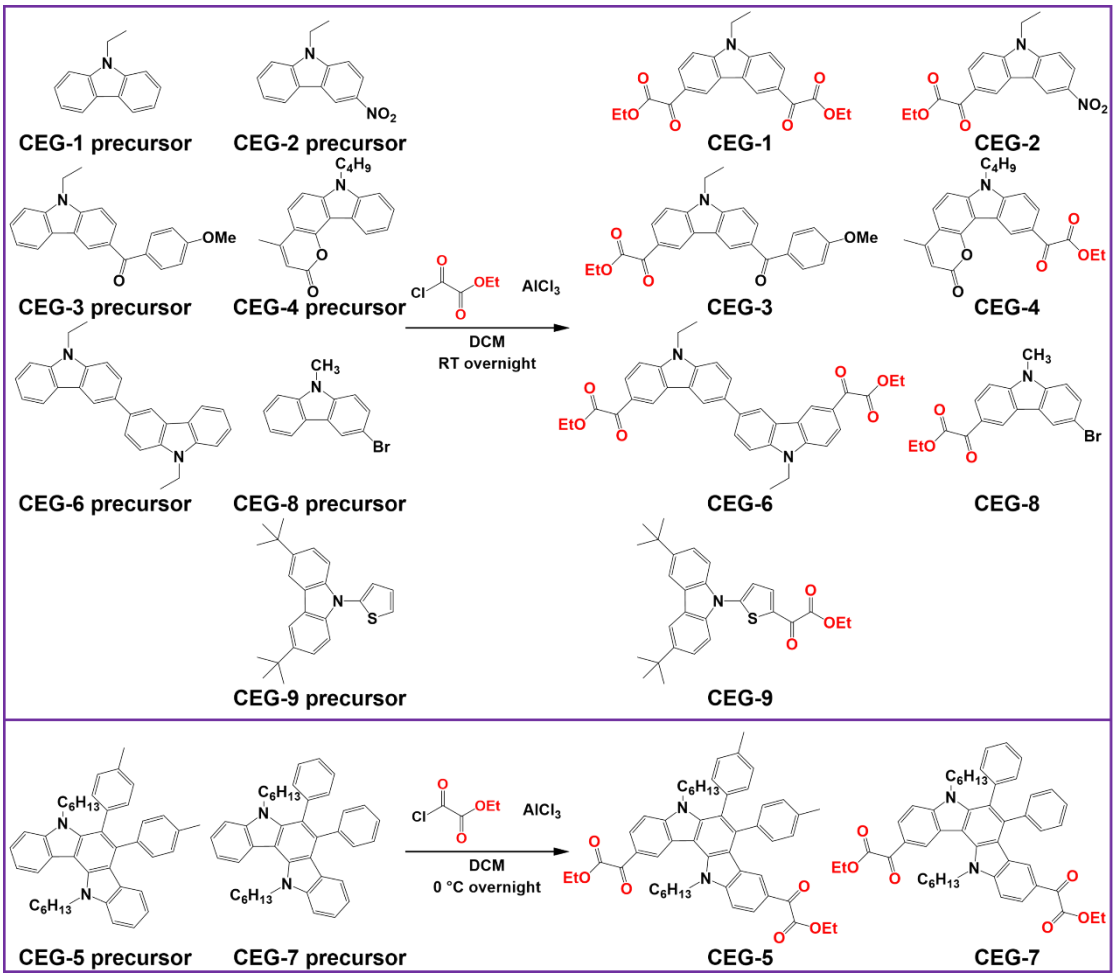

Scheme 2. Synthetic routes to the different CEGs.

Table 1. Final yields (%) for the synthesis of CEGs

CEGs	CEG-1	CEG-2	CEG-3	CEG-4	CEG-5	CEG-6	CEG-7	CEG-8	CEG-9
yield (%)	86	91	77	88	74	89	66	83	92

3.2 Light Absorption Properties

Figure 1 illustrates the UV-visible absorption spectra of CEGs dissolved in acetonitrile. A summary of these optical characteristics of CEGs at the absorption maximum and at 405 nm is given in Table 2. All CEGs exhibited a broad absorption band tailing up to 450 nm, with the exception of CEG-9, where the onset of the absorption spectrum was noticeable at 500 nm. Importantly, the maximum absorption wavelengths (λ_{max}) of all CEGs were above 340 nm, representing a significant redshift compared to the maximum absorption wavelength of MBF (λ_{max} = 266 nm). Notably, the introduction of a strong electron-donating group (i.e. thiophene) in CEG-9 resulted in a substantial redshift of the maximum absorption wavelength, peaking at 406 nm. Additionally, a tail extending up to 500-520 nm was observed for CEG-9, indicating

robust electronic delocalization within this structure. For the carbazole derivatives, electron-withdrawing or electron-donating groups were covalently linked to the carbazole scaffold, slightly influencing the position of the absorption maxima. Notably, electronic delocalization within CEGs could be enhanced by introducing a potent electron accepting group such as a nitro group in CEG-2 (λ_{max} = 366 nm), inducing a push-pull effect between the electron-donating carbazole and the electron-accepting nitro group. Another strategy involved introducing two electron-withdrawing glyoxylate units in CEG-1 (λ_{max} = 356 nm) and CEG-6 (λ_{max} = 353 nm), which also promoted electronic delocalization with the carbazole, despite the relatively weak electron-withdrawing effect of the glyoxylate units. Conversely, the introduction of a halogen in CEG-8 led to a blue shift of the absorption maximum (λ_{max} = 341 nm) compared to the other compounds. Furthermore, extending the π-conjugation, as demonstrated in CEG-1 by fusing a carbazole unit with a coumarin (λ_{max} = 372 nm), effectively redshifted the absorption maximum. However, this fusion strategy was ineffective for CEG-5 and CEG-7, which possessed a 5,12-dihydroindolo[3,2-*a*]carbazole backbone, displaying absorption maxima at 343 and 342 nm, respectively. Despite this, due to the polyaromaticity of these chemicals, notably high molar extinction coefficients were determined for CEG-5 (28400 $M^{-1}\cdot cm^{-1}$) and CEG-7 (33300 $M^{-1}\cdot cm^{-1}$) at their respective absorption maximum. A similar effect was observed in the benzophenone-carbazole combination CEG-5, which exhibited an absorption maximum at 346 nm. Beneficial effect of the extended π-conjugation was confirmed for CEG-6 (ε = 25900 $M^{-1}\cdot cm^{-1}$) and CEG-3 (ε = 21700 $M^{-1}\cdot cm^{-1}$), based on a carbazole dimer and a carbazole-benzophenone combination respectively. The absorption performances of CEGs at 405 nm notably surpassed those of MBF, with consistently higher molar extinction coefficients at 405 nm (ε_{405}) compared to MBF. Particularly, CEG-9 displayed the highest molar extinction coefficient (14500 $M^{-1}\cdot cm^{-1}$) at 405 nm. However, lower molar extinction coefficients for the other PIs at 405 nm did not necessarily indicate inferior photoinitiation abilities when exposed to a 405 nm LED. The photoinitiation ability of a photoinitiator depends not only on its light absorption properties but also on factors such as excited states reactivity (e.g. cleavage ability) as well as the ability of the generated radicals to initiate the polymerization process.[26, 32, 33] Figure S1 illustrates the predicted light absorption properties of CEGs (B3LYP/6-31G* level of theory), while Figure S2 shows the contour plots of the highest occupied molecular orbital (HOMO) and the lowest unoccupied molecular orbital (LUMO) covered by the lowest energy transitions of the CEGs. Consequently, based on these results, it is suggested that CEGs are more sensitive to light irradiation than MBF when exposed to a 405 nm LED.

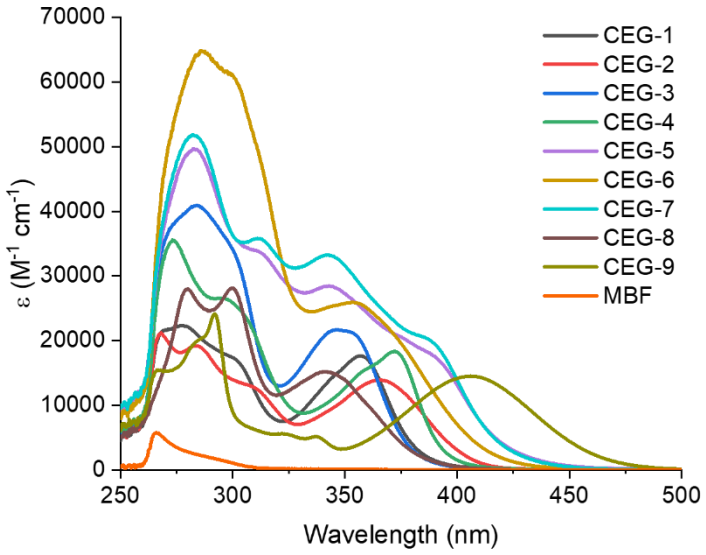

Figure 1. UV-visible absorption spectra of CEGs and MBF in acetonitrile (concentration = 5×10^{-5} M).

Table 2. Light Absorption Properties of CEGs and MBF in acetonitrile (λ_{max} representative of the most red-shifted transition).

PIs	λ_{max} (nm)	ε_{max} ($M^{-1}\cdot cm^{-1}$)	ε_{405} ($M^{-1}\cdot cm^{-1}$)
CEG-1	356	17600	380
CEG-2	366	13900	1900
CEG-3	346	21700	250
CEG-4	372	18300	880
CEG-5	343	28400	10200
CEG-6	353	25900	5200
CEG-7	342	33300	10500
CEG-8	341	15200	320
CEG-9	406	14500	14500
MBF	266	28800	50

3.3 Solubility of CEGs in monomers

PIs reported in the literature often suffered from a poor solubility in monomers. Consequently, methods such as heating, the addition of extra solvents, or ultrasonic treatments were commonly employed to facilitate their dissolutions. However, the use of elevated temperatures and/or ultrasound to dissolve photoinitiators could potentially impact their photoinitiation ability. Additionally, employing solvent to aid photoinitiators dissolution in monomers led to the release of volatile organic compounds (VOC) during photopolymerization, a practice that is no longer considered accepted in current practices. Hence, assessing the solubility of CEGs in TMPTA

became crucial and necessitated investigation (refer to Figure S3). As shown in Table S1, the solubility of CEG-1, CEG-2, CEG-4, and CEG-5 in TMPTA ranged from 0.5 to 5%. Solubility of CEG-7, CEG-8 and CEG-9 exhibited solubility in the range of 5 to 10%, while CEG-3 and CEG-6 showed the solubility in the range of 10 to 20%. Consequently, CEGs synthesized in this study exhibited a good solubility in TMPTA.

3.4 Free Radical Photopolymerization

The photoinitiation ability of CEGs in TMPTA was examined through photopolymerization experiments involving varying molar contents of CEGs and diverse compositions of the multicomponent PISs. The photopolymerization kinetics of TMPTA, triggered by CEGs upon exposure to the 405 nm LED, are depicted in Figure 2. Detailed results, including the final acrylate function conversions (FCs) and the photopolymerization rates (R_p) for various molar contents and formulations, are presented in Tables 3 and 4, along with supplementary information in Tables S2 and S3. Initially, the photoinitiation abilities of CEGs, administered as single-component PISs at concentrations of 1.25×10^{-6} mol·g^{-1}, 2.5×10^{-6} mol·g^{-1}, and 1.25×10^{-5} mol·g^{-1} in TMPTA, were investigated. Subsequently, as the photoinitiation abilities of CEGs in two- and three-component PISs were explored, maintaining CEGs, EDB, and Iod concentration at 1.25×10^{-5} mol·g^{-1} in TMPTA.

For thick samples in single-component PISs, the FCs of most of the CEGs/TMPTA systems increased as the concentrations of CEGs in TMPTA increased from 1.25×10^{-6} mol·g^{-1} to 1.25×10^{-5} mol·g^{-1}. At the same concentration, FCs with CEG-1, CEG-2, CEG-3, and CEG-8 were higher than that of the reference MBF (refer to Figures 2a, 2b, and 2c). For instance, when the concentrations of CEGs were 1.25×10^{-5} mol·g^{-1} TMPTA, the FCs of MBF/TMPTA was 75%, while the FCs of CEG-1/TMPTA, CEG-2/TMPTA, CEG-3/TMPTA, and CEG-8/TMPTA achieved 79, 78, 79, and 81%, respectively, after 600 s of irradiation. Notably, the FCs of CEG-1/TMPTA, CEG-2/TMPTA, CEG-3/TMPTA, and CEG-8/TMPTA reached values close to the maximum after 30 s of the 405 nm LED irradiation, with values of 77, 77, 78, and 80% respectively. These observations indicated that the four CEGs presented above exhibited excellent photoinitiation abilities.

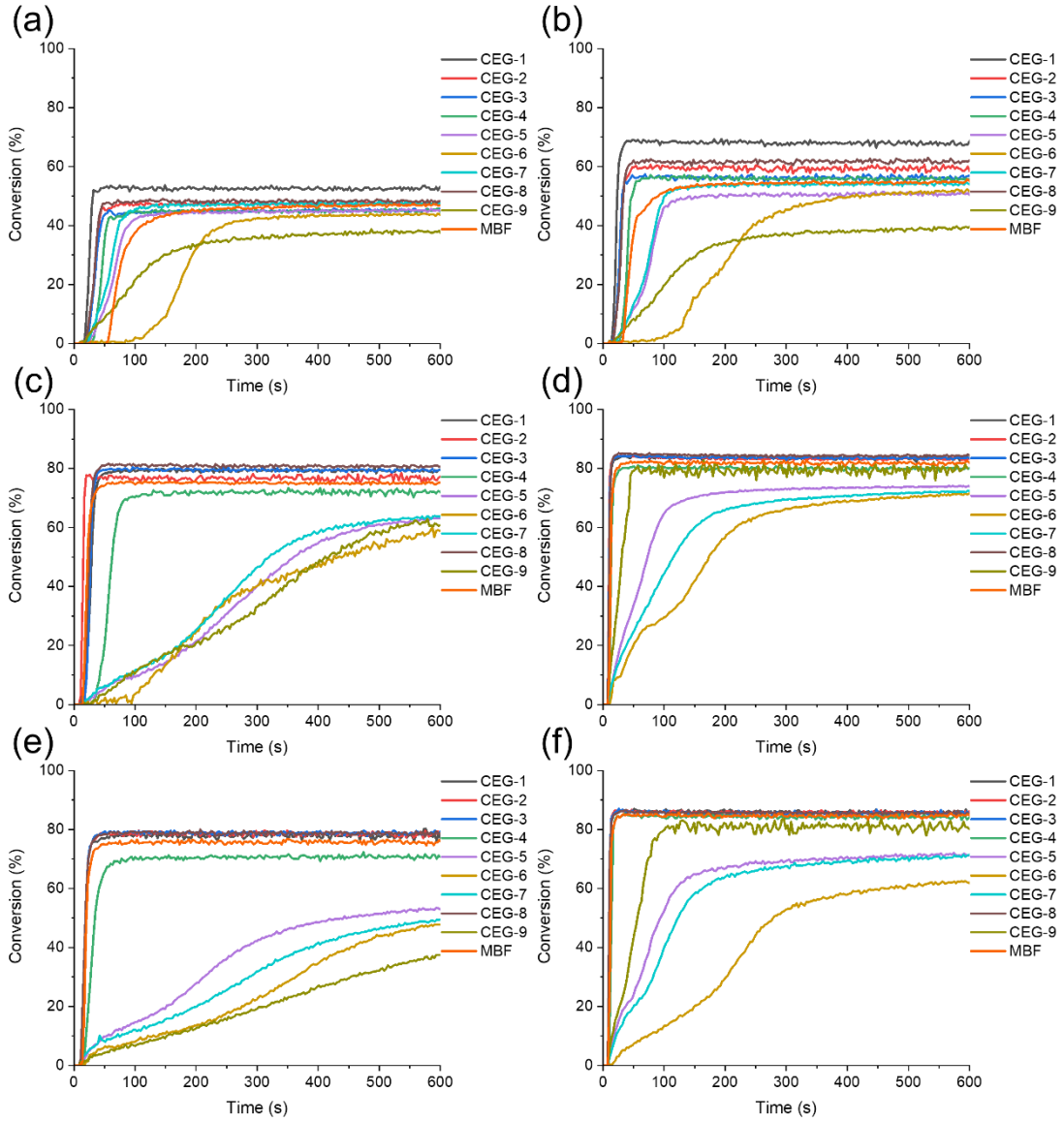

Figure 2. Photopolymerization kinetics of TMPTA in a mold (thickness = 1.4 mm) irradiated by a 405 nm LED under air conditions with photoinitiators: (a) CEGs (1.25×10^{-6} mol·g^{-1} TMPTA); (b) CEGs (2.5×10^{-6} mol·g^{-1} TMPTA); (c) CEGs (1.25×10^{-5} mol·g^{-1} TMPTA); (d) CEGs/EDB (1.25×10^{-5} mol·g^{-1} TMPTA); (e) CEGs/Iod (1.25×10^{-5} mol·g^{-1} TMPTA); (f) CEGs/EDB/Iod (1.25×10^{-5} mol·g^{-1} TMPTA). TMPTA as the monomer. The irradiation starts at t = 10 s.

First of all, a remarkable Type I photoinitiator behavior is found using CEG alone in TMPTA (Figure 2a,2b,2c and SI: Figure S4). Depending of the conditions, their performance can be much better than MBF (See Figure 2a for CEG-1 for example).

For thick samples in both two- (CEGs/EDB, CEGs/Iod) and three-component (CEGs/EDB/Iod) PISs containing CEG-1, CEG-2, CEG-3, and CEG-8, the TMPTA conversions were higher than those obtained with the corresponding two- and three-component PISs containing MBF (refer to Figure 2d, 2e, and 2f). For example, the FCs

of CEG-2/EDB/TMPTA, CEG-2/Iod/TMPTA and CEG-2/EDB/Iod/TMPTA were 83, 79, and 86%, respectively. Likewise, the FCs of CEG-3/EDB/TMPTA, CEG-3/Iod/TMPTA, and CEG-3/EDB/Iod/TMPTA were 84, 79, and 86%, respectively. In contrast, the FCs of MBF/EDB/TMPTA, MBF/Iod/TMPTA, and MBF/EDB/Iod/TMPTA were 82, 76, and 84%, respectively. In both two- (CEGs/EDB) and three-component (CEGs/EDB/Iod) PISs, the FCs of TMPTA were higher than that of TMPTA in single-component (CEGs) PISs. The FCs of TMPTA in some two-component (CEGs/Iod) PISs also increased in the presence of Iod. The Rp of different concentrations and formulations of TMPTA exhibited a similar trend to the corresponding FCs. The above results illustrated that the addition of EDB, Iod, and EDB/Iod can enhance the initiation performance of the photoinitiators.

For thin samples in single-component (CEGs alone) PISs, the FCs of TMPTA were in the range of 53-68% when the concentration of CEGs was 1.25×10^{-5} mol·g^{-1} TMPTA (refer to Figure S4a). Despite the oxygen inhibition effect[13], both the two- and three-component PISs showed good initiation abilities when additives, such as EDB, Iod, and EDB/Iod were added (refer to Figures S4b, S4c, and S4d). Notably, the FCs of TMPTA reached a value as high as 81% when using the CEGs-based three-component PISs, which was greater than that of MBF-based PISs (see Figure S4d). These findings underscored the favorable photoinitiation abilities of the synthesized CEGs when illuminated by the 405 nm LED. In prior reports on glyoxylate derivatives photoinitiators, not only the molar content of PIs used was greater than 1.25×10^{-5} mol·g^{-1} TMPTA, but also the FC of acrylate was lower than the conversion obtained for TMPTA in the study[5, 26]. Among CEGs, CEG-1, CEG-2, CEG-3, and CEG-8 showed superior photoinitiation abilities than the previously reported structures in the literature. Notably, all CEGs can be used in both two- and three component PISs and exhibited promising photoinitiation abilities.

Moreover, the results obtained in this study suggested that the electronic effects[26, 45] of substituents on glyoxylates played a significant role in the photoinitiation ability of CEGs. Electron-donating substituents such as thiophene (for CEG-9) could decrease the photoinitiation ability of CEGs, while the electron-withdrawing substituents could enhance the photoinitiation ability of CEGs (for e.g., CEG-2 and CEG-8).

Table 3. Final acrylate function conversions (FCs) of TMPTA (thick samples) under air conditions with different molar content of PIs in TMPTA after 600 s of irradiation by a 405 nm LED.

1.25×10^{-6} mol·g^{-1}	FC (%)	2.5×10^{-6} mol·g^{-1}	FC (%)	1.25×10^{-5} mol·g^{-1}	FC (%)
CEG-1	53	CEG-1	69	CEG-1	79
CEG-2	48	CEG-2	61	CEG-2	78
CEG-3	48	CEG-3	57	CEG-3	79

CEG-4	45	CEG-4	56	CEG-4	71
CEG-5	45	CEG-5	51	CEG-5	63
CEG-6	44	CEG-6	52	CEG-6	60
CEG-7	48	CEG-7	54	CEG-7	62
CEG-8	48	CEG-8	62	CEG-8	81
CEG-9	38	CEG-9	40	CEG-9	54
MBF	47	MBF	55	MBF	75

Table 4. Final acrylate function conversions (FCs) of TMPTA (thick samples) after 600 s of irradiation by a 405 nm LED under air conditions using the same molar content (1.25×10^{-5} mol·g^{-1} TMPTA) of PIs, EDB and Iod.

PIs	FC (%)	PIs/EDB	FC (%)	PIs/Iod	FC (%)	PIs/EDB/Iod	FC (%)
CEG-1	79	CEG-1	83	CEG-1	79	CEG-1	85
CEG-2	78	CEG-2	83	CEG-2	79	CEG-2	86
CEG-3	79	CEG-3	84	CEG-3	79	CEG-3	86
CEG-4	71	CEG-4	80	CEG-4	71	CEG-4	84
CEG-5	63	CEG-5	74	CEG-5	53	CEG-5	72
CEG-6	60	CEG-6	72	CEG-6	48	CEG-6	62
CEG-7	62	CEG-7	72	CEG-7	50	CEG-7	71
CEG-8	81	CEG-8	85	CEG-8	79	CEG-8	86
CEG-9	54	CEG-9	75	CEG-9	38	CEG-9	80
MBF	75	MBF	82	MBF	76	MBF	84

3.5 Decarboxylation mechanism

In the course of photopolymerization experiments, the occurrence of a decarboxylation reaction was assessed by RT-FTIR detection of CO_2 production (refer to Figure 3). The RT-FTIR spectra of CEG-1, CEG-2, CEG-3, and CEG-8 revealed a distinctive new absorption peak of CO_2 at 2337 cm^{-1} during the photopolymerization process (refer to Figures 3a, 3b, 3c, and 3d). However, the extend of the decarboxylation reaction depends of the CEG structure (See Figure S5). Meanwhile, it was found that there was no new infrared absorption peak of CO at 2143 cm^{-1} during t = 0 s and t = 60 s (refer to Figures 3a, 3b, 3c, 3d, Figures S5), signifying that no CO was generated during the photopolymerization process. These findings can validate the occurrence of decarboxylation during the photopolymerization process, which meant that the PIs decomposed and generated free radicals to initiate the photopolymerization of TMPTA under the irradiation of the 405 nm LED.

Moreover, apart from examining the CO_2 absorption intensity versus irradiation time (see Figure 3e), the relationship between CO_2 absorption intensity, conversion rate, and irradiation time was also investigated (see Figure 3f). As shown in Figure 3e, from t = 10 s to t = 20 s, the absorbance of CO_2 in the photoinitiating systems involving CEG-

2 and CEG-3 exhibited a rapid surge, in direct correlation with the production of CO_2 through the decarboxylation process. Post t = 50 s, the CO_2 absorbance of plateaued or displayed minimal incremental changes. This trend corresponded with the swift rise in the functional conversions of acrylates within the CEG-2 and CEG-3 systems during the irradiation period, indicating a close relationship between the generation of CO_2 and the progression of functional conversions of acrylates. A similar behavior was found for oxime-ester photoinitiators for which decarboxylation reactions also occur.[46]

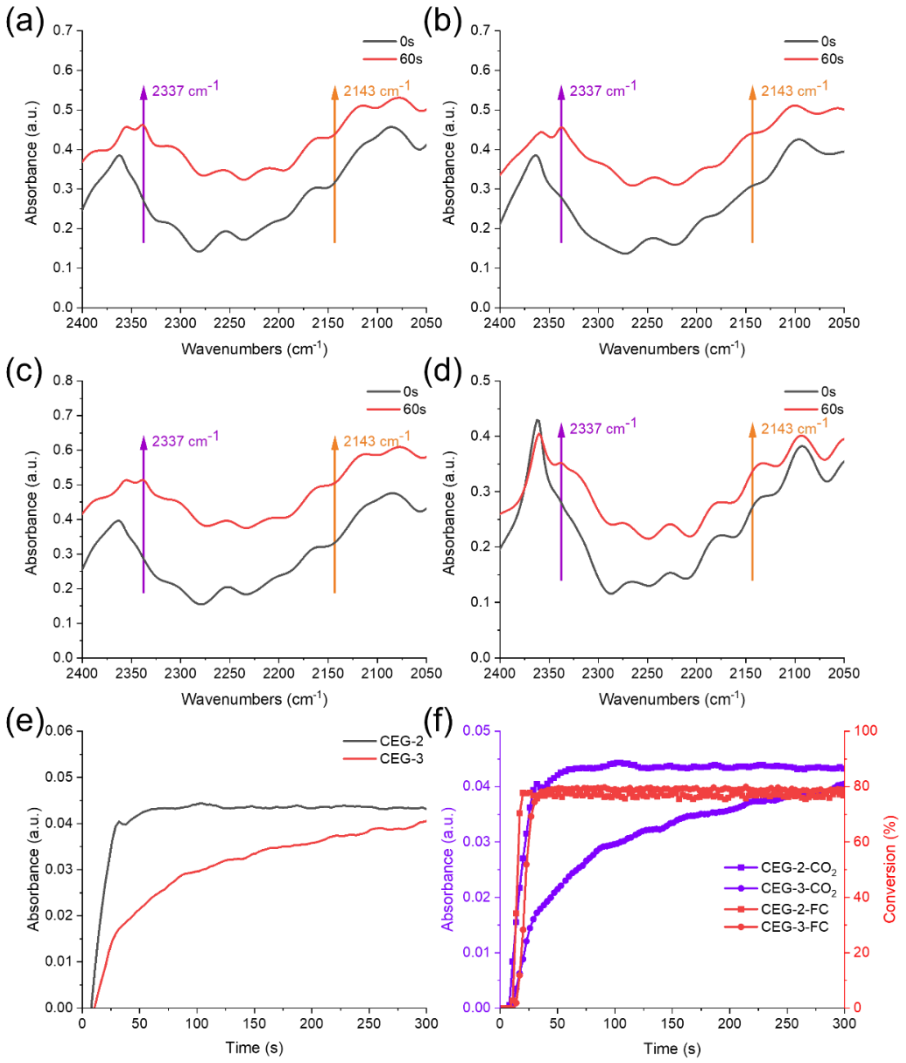

Figure 3. Infrared spectra of (a) CEG-1, (b) CEG-2, (c) CEG-3, and (d) CEG-8 in TMPTA at t = 10 s and 60 s. (e) The curves of absorption intensity of CO_2 derived from CEG-2 and CEG-3 (the irradiation starts for t = 10s). (f) The curves of absorption intensity of CO_2 released and functional conversions (acrylate functions conversions vs irradiation time) derived from CEG-2 and CEG-3.

3.5 Photochemistry of CEGs

To unveil the photochemical mechanism underlying CEGs, steady-state photolysis experiments were conducted in both acetonitrile and TMPTA, exposing CEGs solutions

to a 405 nm LED under ambient air conditions. Figure 4 presents the steady-state photolysis of CEG-1, CEG-2, CEG-3, and CEG-8 in acetonitrile. The intensity of the absorption peaks of CEG-1 and CEG-2 showed a delayed decrease after 1800 s of irradiation with the 405 nm LED (refer to Figures 4a and 4b). In contrast, the absorption peaks of CEG-3 and CEG-8 showed minimal decline after irradiated by the 405 nm LED for 1800 s (see Figures 4c and 4d). Similar trends were observed for other CEGs, displaying negligible change of absorption in acetonitrile, which closely paralleled the photolysis behavior of CEG-2 and CEG-8 (see Figure S6). Two plausible explanations could account for these experimental observations. The first possibility was that CEG-3 and CEG-8 may not cleave when exposed to the 405 nm LED or in photoproducts exhibiting very similar light absorption properties. The second rationale could be attributed to the cage effect of the solvent in the solution.[25, 47] Subsequently, CEG-1, CEG-2, CEG-3, and CEG-8 underwent steady-state photolysis in TMPTA. Figure 5 illustrates a substantial decrease in the intensity of the absorption peaks of CEG-1, CEG-2, CEG-3, and CEG-8 over extended irradiation periods in TMPTA compared to those observed in acetonitrile. In contrast to the photolysis results in acetonitrile, the photolysis findings of other CEGs in TMPTA turn out to be quite impressive, showing remarkable similarity to those of CEG-1, CEG-2, CEG-3, and CEG-8 in TMPTA (refer to Figure S7). Markedly, in TMPTA, isobestic points (~330-340 nm) are found clearly suggesting a clean cleavage process without other side-reactions. Combining the decarboxylation and photolysis experiments, it was evident that CEGs generated free radicals for photopolymerization with TMPTA under the irradiation of 405 nm LED (also confirmed below by the ESR results).

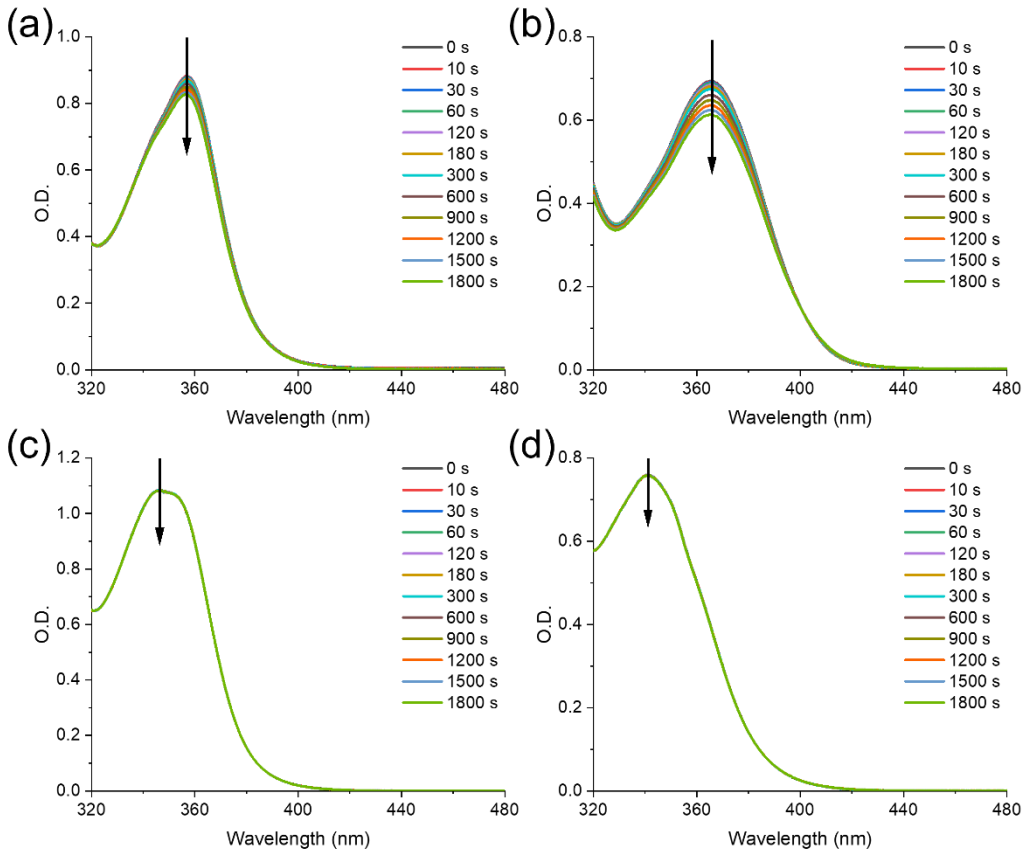

Figure 4. Steady-state photolysis of (a) CEG-1, (b) CEG-2, (c) CEG-3, and (d) CEG-8 in acetonitrile when exposed to the 405 nm LED (concentration = 5×10^{-5} M).

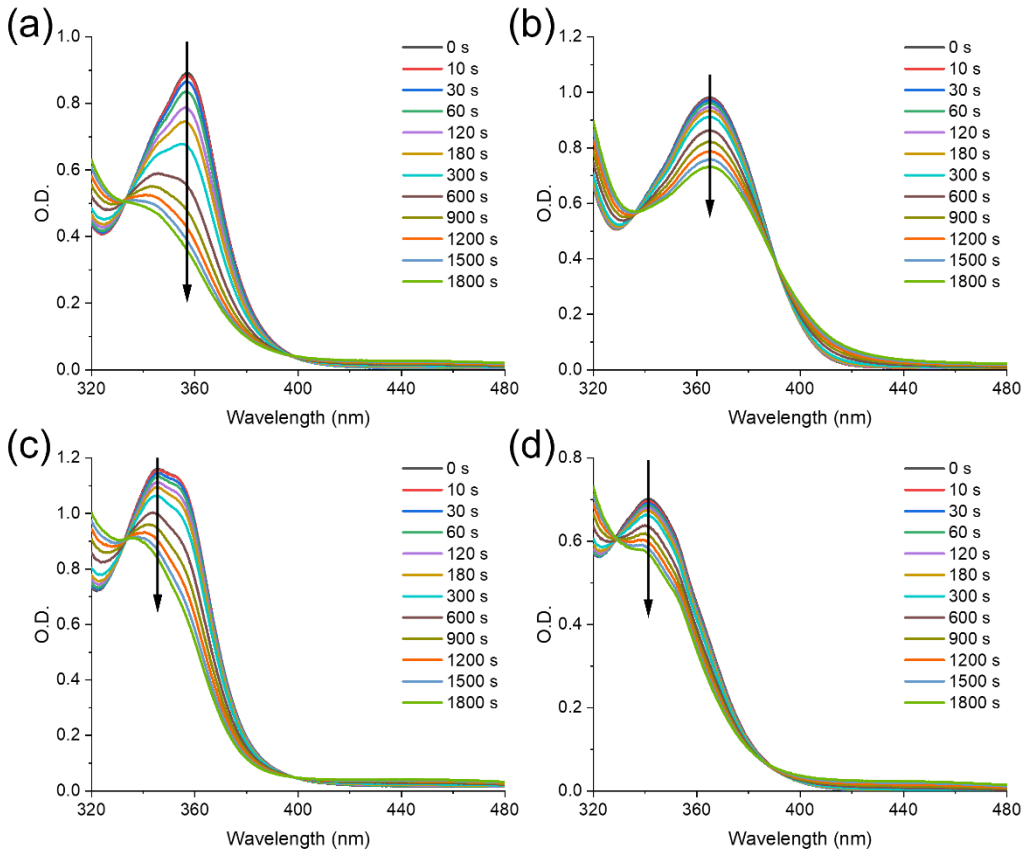

Figure 5. Steady-state photolysis of (a) CEG-1, (b) CEG-2, (c) CEG-3, and (d) CEG-8 in TMPTA when exposed to the 405 nm LED (concentration = 5×10^{-5} M).

Additionally, the fluorescence lifetimes of CEG-2, CEG-3, and other CEGs were evaluated (refer to Table S4). The response time of the instrument (1.4 ns) exceeded the fluorescence lifetime of most of the CEGs described above. Thus, it was inherent characteristic of the carbazole-containing chromophore that such short fluorescence lifetimes were observed. Such brevity in fluorescence lifetime can suggest a fast and efficient cleavage in the excited states that typically contributes to a rapid initiation of the reaction. Markedly, CEG-2, CEG-3 and CEG-8 that correspond to the best Type I photoinitiators are also characterized by the shortest singlet excited state lifetimes (Table S4) in agreement with their better cleavage ability from S_1. According to existing literature,[48] the singlet state energy (E_{S1}) of CEG-2 and CEG-3 were determined from the intersection of the normalized UV-visible absorption and fluorescence spectra as shown in Figures 6a and 6b. The results of the singlet state energy determination for the other CEGs are displayed in Figure S8.

For all CEGs, two radical adducts (radicals trapped by PBN) were found in ESR spin-trapping experiments with hyperfine coupling constants aN = 14.0 G and aH = 5.4G and aN = 13.3G and aH = 1.7G, respectively. These structures can correspond to

acyl (RC(O)°) and oxygen centered radicals (see below) in full agreement with the Type I initiator behavior of CEGs. For example, Figures 6c and 6d present the ESR spectra of CEG-2 and CEG-3 under the 405 nm LED illumination with PBN as the trapping agent.

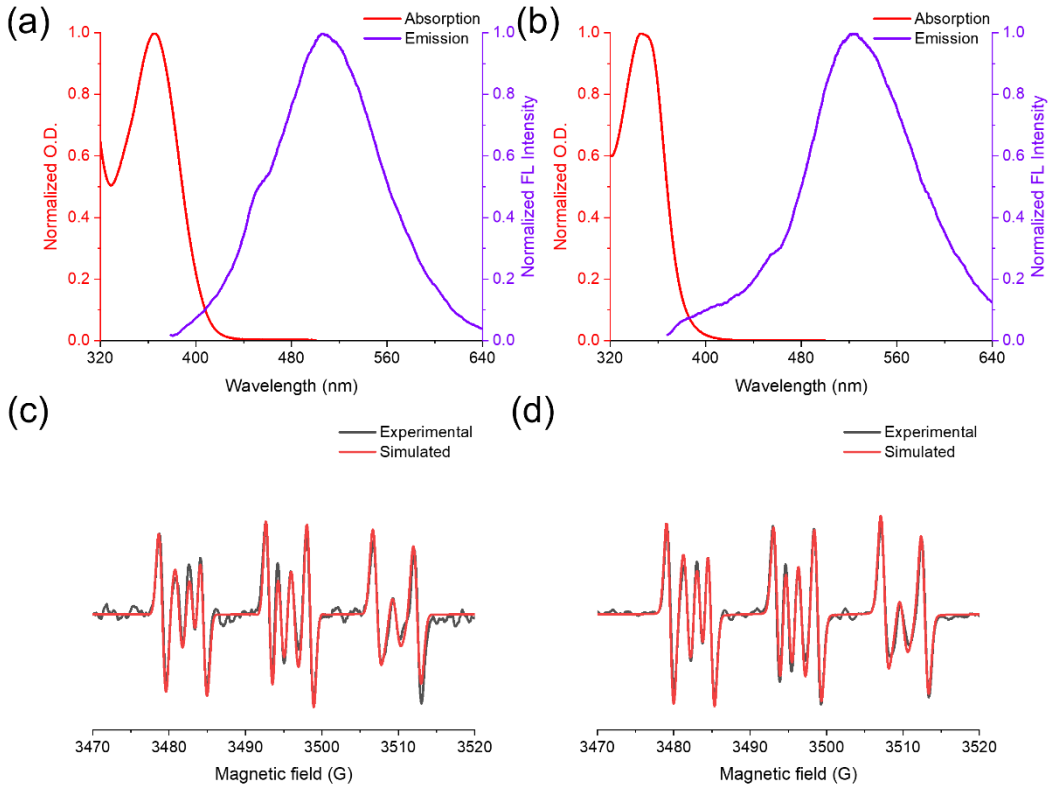

Figure 6. The curves of singlet state energy determination of (a) CEG-2 and (b) CEG-3. ESR-ST spectra of the radical adducts of (c) CEG-2 and (d) CEG-3 in N_2 saturated medium when exposed to the 405 nm LED, with PBN acting as the trapping agent in *tert*-butylbenzene.

Considering the three different possible cleavage processes from the C-C or C-O Bond Dissociation Energies evaluated by DFT calculations (Scheme 3 for CEG-2), the cleavages of the central C(=O)-C(=O) (refer to pathway 1 in Scheme 4) or C-O bond (refer to pathway 2 in Scheme 4) can be suspected. Indeed, the third bond (with BDE = 92.6 kcal/mol) is too high in energy i.e. much higher than the excited state energy to be cleaved.

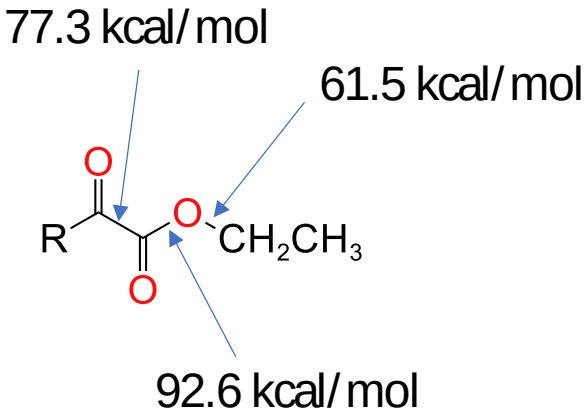

Scheme 3. Bond Dissociation Energies calculated in the glyoxylate chromophore.

Enthalpy ΔH for the cleavage process of the C-C and C-O bonds from either the singlet state (S_1) or triplet state (T_1) was calculated for CEG-2 using the equation $\Delta H_{\text{cleavage S1(or T1)}}$ = BDE(C-C or C-O) - E_{S1} (or E_{T1}), as outlined in Table 5. Interestingly, the C-O cleavage from S_1 is found favorable ($\Delta H_{\text{cleavage}} < 0$). However, when the value of $\Delta H_{\text{cleavage S1}}$ was positive ($\Delta H_{\text{cleavage}} > 0$ for C-C cleavage from both S_1 and T_1 or C-O from T_1), the cleavage reaction can occur if the enthalpy value was not the sole determinant for the occurrence of the cleavage reaction i.e. more particularly if the decarboxylation favors the process. In this latter context; the decarboxylation of •C(=O)OEt is calculated here very favorable (-13.6 kcal/mol) in pathway 1 (see Scheme 4). A same behavior is found for the carbazole-glyoxylate radical (R-C(=O)C(=O)O•) in pathway 2 (Scheme 4).

Table 5. C-C or C-O Bond Dissociation Energies (BDE), E_{S1}, E_T, $\Delta H_{\text{cleavage S1}}$, $\Delta H_{\text{cleavage T1}}$ of CEG-2.

Pathway 1				
C-C BDE (kcal mol^{-1})	E_{S1} (kcal mol^{-1})	$\Delta H_{\text{cleavage S1}}$ (kcal mol^{-1})	E_T (kcal mol^{-1})	$\Delta H_{\text{cleavage T1}}$ (kcal mol^{-1})
77.31	70.09	7.22	55.46	21.85
Pathway 2				
C-O BDE (kcal mol^{-1})	E_{S1} (kcal mol^{-1})	$\Delta H_{\text{cleavage S1}}$ (kcal mol^{-1})	E_T (kcal mol^{-1})	$\Delta H_{\text{cleavage T1}}$ (kcal mol^{-1})
61.5	70.09	-8.59	55.46	6.04

As shown in Scheme 4, the potential photolysis mechanisms of CEGs[5, 26, 49] has been proposed based on the aforementioned results. CEGs generated free radicals through two distinct ways (noted (1) and (2) in Scheme 4) when exposed to the 405 nm

LED. In the presence of monomers in the system, these free radicals demonstrated the ability to initiate their polymerization. Specifically, the polymerization of TMPTA monomers can be initiated through two pathways when irradiated by the 405 nm LED. Firstly, the C-C bond between the dicarbonyl groups dissociated to produce substituted carbazolecarbonyl radicals and ethoxycarbonyl radicals (pathway 1 in Scheme 4). Subsequent decarboxylation of the ethoxycarbonyl radicals led to the formation ethyl radical and CO_2. Secondly, the cleavage of the C-O bond between the ethoxy groups generated substituted carbazole glyoxylate radical and ethyl radical (pathway 2 in Scheme 4). Following this, the substituted carbazole glyoxylate radical can undergo decarboxylation to generate carbazolecarbonyl and CO_2. In both case (pathways 1 or 2), both carbazolecarbonyl radicals and ethyl radicals can initiate polymerization of acrylate monomers.

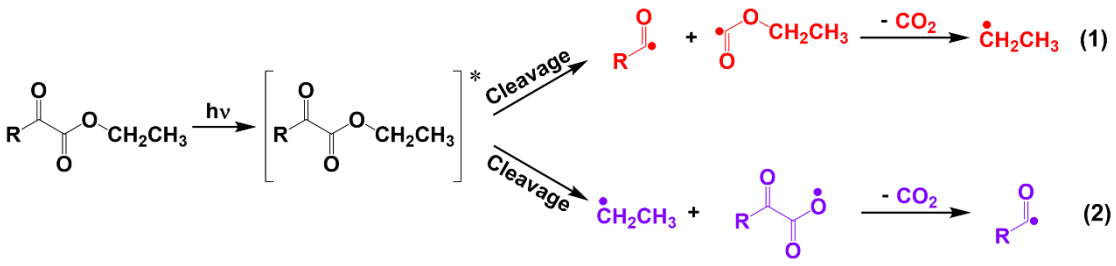

Scheme 4. Potential photoinitiation mechanism of CEGs.

3.6 3D Printing

Because of the good photoinitiation properties of CEG-2 and CEG-3 in the preceding photopolymerization experiments, CEG-2 and CEG-3 were selected as ideal candidates for the design of prototype systems intended for 3D printing. As illustrated in Figure 8, successful execution of 3D printing and direct laser write (DLW) experiments was achieved. The concentration of both CEG-2 and CEG-3 was 1.25×10^{-5} mol·g^{-1} in TMPTA. During the 3D printing experiments, a 3D object mesh cubic box (20 mm in length and width, 10 mm in height) was successfully printed using a DLP 3D printer (Anycubic Photon D2 at 405 nm) with a computer design model (refer to Figures 7a - 7e). Subsequent observation of the 3D printed objects using a scanning electron microscope (SEM) revealed their morphological completeness and high resolution (refer to Figures 7f, 7g, and 7h). Meanwhile, in the DLW experiments, the letter patterns “SKY” (with a thickness of approximately 2800 μm) were fabricated within a short duration (approximately 2 mins) using a 405 nm laser diode (Thorlabs, UK) (refer to Figure 7i). These patterns were subsequently examined using a numerical optical microscope (refer to Figure 7j), which confirmed the high spatial resolution of

the 3D objects. Whether employed for 3D printing or DLW, CEGs have unequivocally demonstrated their efficiency as photoinitiators.

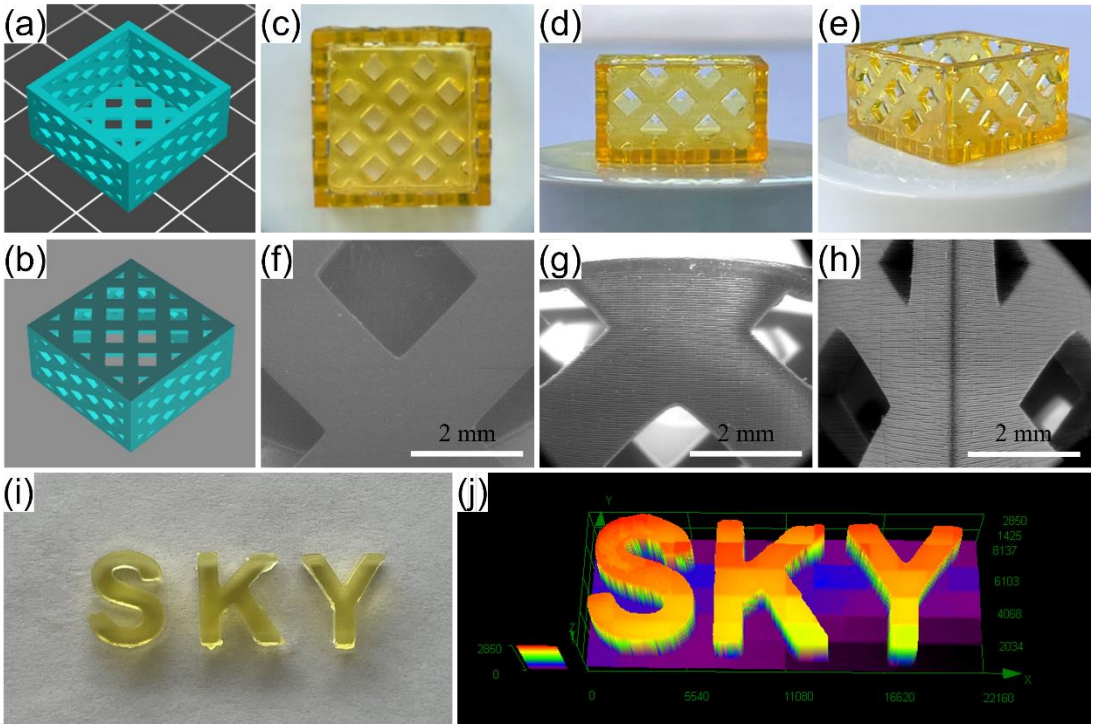

Figure 7. (a) and (b) Computer model; 3D printed object obtained from CEG-2/TMPTA. Three views: (c) top, (d) lateral, and (e) oblique; SEM image of the 3D printed object obtained from CEG-2/TMPTA (scale bar = 2 mm). Three views: (f) top, (g) lateral, and (h) oblique; (i) direct laser write object obtained from CEG-3/TMPTA; (j) numerical optical microscopy characterization of the 3D objects obtained from CEG-3/TMPTA.

3.7 Chemical mechanisms in multicomponent systems

For CEG/EDB or CEG/EDB/Iod, the initiating ability can be improved compared to CEG alone i.e. the following trend of reactivity is observed CEG/EDB/Iod > CEG/EDB > CEG ~ CEG/Iod. The expected mechanisms are given below in Scheme 5 and correspond to an electron transfer reaction leading to aminoalkyles (for EDB) radicals as initiating species. Such a dual Type I/Type II behavior has been already mentioned for MBF in previous works.[50, 51] In fluorescence quenching experiments, a clear interaction is found between ^{1}CEG and EDB as a new fluorescence photoproduct was detected (Figures S9a and S9b). Unfortunately, this new fluorescence prevents only Stern-Volmer quenching determination. For ^{1}CEG/Iod, no fluorescence quenching was observed (Figures S9b and S9d). Therefore, for the excited states of CEG (CEG*), the Type I photoinitiator behavior (r1, see also Scheme 4) is now in competition with the interaction with the additives (EDB (r2)). For the three-component systems (CEG/EDB/Iod), r3 can also probably occur as in many three-component systems

increasing the initiation radical yields and hence improving the polymerization initiating abilities.[50]

$$CEG\ (h\nu) \rightarrow CEG^* \rightarrow Radicals \quad (r1)$$

$$CEG^* + EDB \rightarrow CEG\text{-}H^{\bullet} + EDB^{\bullet}_{(-H)} \quad (r2)$$

$$CEG\text{-}H^{\bullet} + Ar_2I^{+} \rightarrow CEG + H^{+} + Ar^{\bullet} + Ar\text{-}I \quad (r3)$$

Scheme 5. Proposed Type I vs. multicomponent mechanisms in CEG.

4. Conclusions

Nine CEGs were successfully designed and synthesized as innovative PIs tailored for LED-induced photopolymerization, featuring the ethyl glyoxylate moiety as the end group. The incorporation of the carbazole group in these compounds resulted in a notable redshifted absorption compared to the reference MBF, showcasing outstanding light absorption capabilities in the near-UV and visible region. Under 405 nm with a LED, CEGs produced initiating radicals, which were accompanied by decarbonylation reaction. CEGs showed exceptional photoinitiation properties for free radical polymerization across single-, two- and three-component PISs when subjected to 405 nm LED irradiation. Specifically, CEG-1, CEG-2, CEG-3, and CEG-8 outperformed commercial PI MBF in both mono- and multi-component PISs. The presence of electron-donating substituents weakened the photoinitiation ability of CEGs, while electron-withdrawing substituents enhanced their photoinitiation ability. Notably, the successful application of CEGs in laser direct write and 3D printing solidified their excellent photoinitiation abilities. Consequently, the CEGs investigated in this study exhibit promising development prospect and substantial application potential in photopolymerization materials. Moreover, they present a viable strategy for the advancement of novel photoinitiators within the field.

Acknowledgements

This research project is supported by China Scholarship Council (CSC) (No.202206340021). This work was performed using HPC resources of the Mesocentre of the University of Strasbourg and the HPC resources from GENCI-IDRIS (Grant 2023-AD010812313R2 /Jean_Zay).

References

1 K. Kostrzewska, J. Ortyl, R. Dobosz, J. Kabatc, *Polym. Chem.* 2017, ***8***, 3464.

2 J. Kirschner, F. Szillat, M. Bouzrati-Zerelli, J. M. Becht, J. E. Klee, J. Lalevee, *J. Polym. Sci., Part A: Polym. Chem.* 2019, ***57***, 1664.

3 P. Garra, J. P. Fouassier, S. Lakhdar, Y. Yagci, J. Lalevee, *Prog. Polym. Sci.* 2020, ***107***, 101277.

4 H. Mokbel, D. Anderson, R. Plenderleith, C. Dietlin, F. Morlet-Savary, F. Dumur, D. Gigmes, J. P. Fouassier, J. Lalevee, *Polym. Chem.* 2017, ***8***, 5580.

5 M. Bouzrati-Zerelli, J. Kirschner, C. P. Fik, M. Maier, C. Dietlin, F. Morlet-Savary, J. P. Fouassier, J. M. Becht, J. E. Klee, J. Lalevee, *Macromolecules* 2017, ***50***, 6911.

6 Y. P. Wu, R. Li, J. W. Wang, Y. Situ, H. Huang, *J. Polym. Sci.* 2022, ***60***, 52.

7 X. Kuang, J. T. Wu, K. J. Chen, Z. Zhao, Z. Ding, F. J. Y. Hu, D. N. Fang, H. J. Qi, *Sci. Adv.* 2019, ***5***, eaav5790.

8 M. B. Sponsler, *J. Phys. Chem.* 1995, ***99***, 9430.

9 Y. P. Wu, R. Li, J. S. Ke, X. Cheng, R. Tang, Y. Situ, H. Huang, *Eur. Polym. J.* 2022, ***168***, 111093.

10 M. Kara, S. Dadashi-Silab, Y. Yagci, *Macromol. Rapid Commun.* 2015, ***36***, 2070.

11 T. Gong, B. J. Adzima, C. N. Bowman, *Chem. Commun.* 2013, ***49***, 7950.

12 J. Zhang, D. Campolo, F. Dumur, P. Xiao, J. P. Fouassier, D. Gigmes, J. Lalevee, *ChemCatChem* 2016, ***8***, 2227.

13 J. J. Yang, C. Xu, W. Liao, Y. Xiong, X. L. Wang, H. D. Tang, *Prog. Org. Coat.* 2020, ***138***, 105410.

14 S. H. Liu, T. Borjigin, M. Schmitt, F. Morlet-Savary, P. Xiao, J. Lalevee, *Polymers* 2023, ***15***, 342.

15 N. Karaca, D. K. Balta, N. Ocal, N. Arsu, *J. Lumines.* 2014, ***146***, 424.

16 H. Tar, D. S. Esen, M. Aydin, C. Ley, N. Arsu, X. Allonas, *Macromolecules* 2013, ***46***, 3266.

17 J. Zhang, K. Launay, N. S. Hill, D. Zhu, N. Cox, J. Langley, J. Lalevee, M. H. Stenzel, M. L. Coote, P. Xiao, *Macromolecules* 2018, ***51***, 10104.

18 Z. Gomurashvili, J. V. Crivello, *Macromolecules* 2002, ***35***, 2962.

19 W. X. Han, H. Y. Fu, T. L. Xue, T. Z. Liu, Y. Wang, T. Wang, *Polym. Chem.* 2018, ***9***, 1787.

20 J. Zhang, F. Dumur, P. Xiao, B. Graff, D. Bardelang, D. Gigmes, J. P. Fouassier, J. Lalevee, *Macromolecules* 2015, ***48***, 2054.

21 C. Dworak, R. Liska, *J. Polym. Sci., Part A: Polym. Chem.* 2010, ***48***, 5865.

22 F. Dumur, *Eur. Polym. J.* 2022, ***175***, 111330.

23 Y. P. Wu, C. X. Dai, J. S. Ke, R. Tang, C. G. Huang, J. W. Wang, S. T. Yue, H. Huang, *Prog. Org. Coat.* 2023, ***176***, 107396.

24 X. Y. Ma, D. Cao, X. T. Hu, J. Nie, T. Wang, *Prog. Org. Coat.* 2020, ***144***, 105651.

25 J. Yu, Y. J. Gao, S. L. Jiang, F. Sun, *Macromolecules* 2019, ***52***, 1707.

26 X. L. He, Y. J. Gao, J. Nie, F. Sun, *Macromolecules* 2021, ***54***, 3854.

27 F. Hammoud, A. Hijazi, M. Schmitt, F. Dumur, J. Lalevée, *Eur. Polym. J.* 2023, ***188***, 111901.

28 F. Dumur, *Eur. Polym. J.* 2020, ***125***, 109503.

29 T. Aggarwal, Sushmita, A. K. Verma, *Org. Biomol. Chem.* 2019, ***17***, 8330.

30 Z. C. Xu, D. Wu, C. Fang, Y. Z. Li, *Des. Monomers Polym.* 2023, ***26***, 90.

31 L. Allen, P. Natho, *Org. Biomol. Chem.* 2023, ***21***, 8956.

32 D. E. Fast, A. Lauer, J. P. Menzel, A. M. Kelterer, G. Gescheidt, C. Barner-Kowollik, *Macromolecules* 2017, ***50***, 1815.

33 R. C. Zhou, X. Sun, R. Mhanna, J. P. Malval, M. Jin, H. Y. Pan, D. C. Wan, F. Morlet-Savary, H.

Chaumeil, C. Joyeux, *ACS Appl. Polym. Mater.* 2020, ***2***, 2077.
34 L. Deng, J. Q. Qu, *Prog. Org. Coat.* 2023, ***183***, 107766.
35 S. H. Liu, N. Giacoletto, M. Schmitt, M. Nechab, B. Graff, F. Morlet-Savary, P. Xiao, F. Dumur, J. Lalevée, *Macromolecules* 2022, ***55***, 2475.
36 S. H. Liu, H. Chen, Y. J. Zhang, K. Sun, Y. Y. Xu, F. Morlet-Savary, B. Graff, G. Noirbent, C. Pigot, D. Brunel, M. Nechab, D. Gigmes, P. Xiao, F. Dumur, J. Lalevée, *Polymers* 2020, ***12***, 1394.
37 K. B. Zheng, W. Y. Lin, L. Tan, H. Chen, H. J. Cui, *Chem. Sci.* 2014, ***5***, 3439.
38 A. Et Taouil, S. Lakard, F. Dumur, E. Contal, B. Lakard, *Synth. Met.* 2023, ***300***, 117491.
39 F. Hammoud, A. Hijazi, S. Duval, J. Lalevée, F. Dumur, *Eur. Polym. J.* 2022, ***162***, 110880.
40 M. Ben Braiek, F. Aloui, S. Moussa, M. Tounsi, J. Marrot, B. Ben Hassine, *Tetrahedron Lett.* 2013, ***54***, 5421.
41 K. Gräf, M. A. Rahim, S. Das, M. Thelakkat, *Dyes Pigm.* 2013, ***99***, 1101.
42 V. Nair, V. Nandialath, K. G. Abhilash, E. Suresh, *Org. Biomol. Chem.* 2008, ***6***, 1738.
43 N. A. Kazin, N. S. Demina, R. A. Irgashev, E. F. Zhilina, G. L. Rusinov, *Tetrahedron* 2019, ***75***, 4686.
44 R. C. Zhou, J. P. Malval, M. Jin, A. Spangenberg, H. Y. Pan, D. C. Wan, F. Morlet-Savary, S. Knopf, *Chem. Commun.* 2019, ***55***, 6233.
45 E. Shin, C. Lim, U. J. Kang, M. Kim, J. Park, D. Kim, W. Choi, J. Hong, C. Baig, D. W. Lee, B. S. Kim, *Macromolecules* 2020, ***53***, 3551.
46 F. Hammoud, N. Giacoletto, G. Noirbent, B. Graff, A. Hijazi, M. Nechab, D. Gigmes, F. Dumur, J. Lalevee, *Mat. Chem. Front.* 2021, ***5***, 8361.
47 C. H. Tung, Y. M. Ying, *Res. Chem. Intermed.* 1998, ***24***, 15.
48 C. Dietlin, T. T. Trinh, S. Schweizer, B. Graff, F. Morlet-Savary, P. A. Noirot, J. Lalevee, *Macromolecules* 2019, ***52***, 7886.
49 H. Y. Pan, S. Q. Chen, M. Jin, J. P. Malval, D. C. Wan, F. Morlet-Savary, *Polym. Chem.* 2019, ***10***, 1599.
50 J. P. Fouassier, J. Lalevee, *Photoinitiators for Polymer Synthesis: Scope, Reactivity and Efficiency*, Wiley-VCH Verlag GmbH, Weinheim 2012.
51 J. P. Fouassier, J. Lalevee, *Photoinitiators: Structures, Reactivity and Applications in Polymerization*, WILEY-VCH GmbH, Weinheim 2021.

TOC graphic:

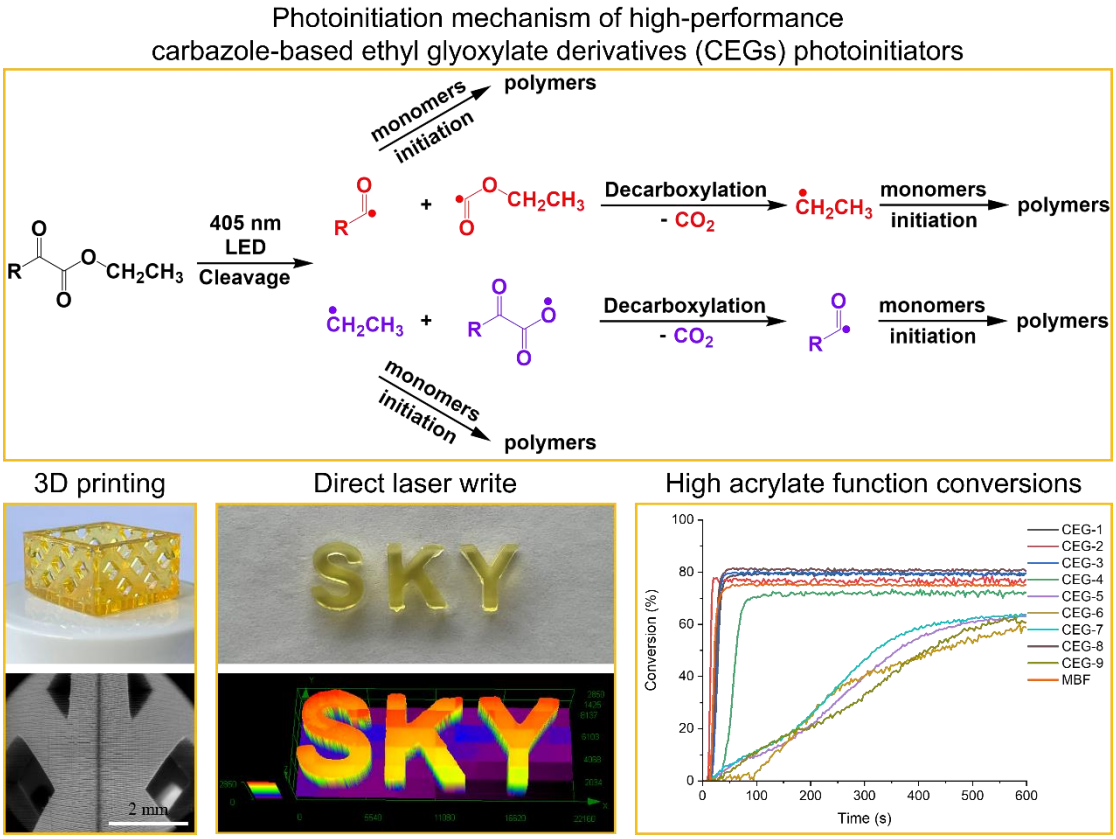
Photoinitiation mechanism of high-performance
carbazole-based ethyl glyoxylate derivatives (CEGs) photoinitiators
monomers
initiation
polymers
405 nm
LED
Cleavage
Decarboxylation
- CO2
monomers
initiation
polymers
Decarboxylation
- CO2
monomers
initiation
polymers
monomers
initiation
polymers
3D printing
Direct laser write
High acrylate function conversions
2 mm
SKY
SKY
Conversion (%)
Time (s)
CEG-1
CEG-2
CEG-3
CEG-4
CEG-5
CEG-6
CEG-7
CEG-8
CEG-9
MBF